Acta Pharmaceutica Sinica B 2024;14(9):4087−4101

Chinese Pharmaceutical Association
Institute of Materia Medica, Chinese Academy of Medical Sciences

Acta Pharmaceutica Sinica B

www.elsevier.com/locate/apsb
www.sciencedirect.com

ORIGINAL ARTICLE

Mitochondrial metabolism blockade nanoadjuvant reversed immune-resistance microenvironment to sensitize albumin-bound paclitaxel-based chemo-immunotherapy

Zaigang Zhou [a,†], Wenjuan Luo [b,†], Chunjuan Zheng [b,†], Haoxiang Wang [a], Rui Hu [d], Hui Deng [b,*], Jianliang Shen [a,c,*]

[a]*National Engineering Research Center of Ophthalmology and Optometry, Eye Hospital, Wenzhou Medical University, Wenzhou 325027, China*
[b]*School & Hospital of Stomatology, Wenzhou Medical University, Wenzhou 325027, China*
[c]*Zhejiang Engineering Research Center for Tissue Repair Materials, Wenzhou Institute, University of Chinese Academy of Sciences, Wenzhou 325001, China*
[d]*Department of the Second Affiliated Hospital of Wenzhou Medical University, Wenzhou 325000, China*

Received 3 February 2024; received in revised form 15 May 2024; accepted 17 May 2024

KEY WORDS

Chemo-immunotherapy;
Collagen;
Transforming growth factor-β;
Mitochondrial metabolism;
Programmed cell death-ligand 1;
Drug accumulation;
Albumin-bound paclitaxel;
Immune-resistance microenvironment

Abstract Currently, the efficacy of albumin-bound paclitaxel (PTX@Alb) is still limited due to the impaired PTX@Alb accumulation in tumors partly mediated by the dense collagen distribution. Meanwhile, acquired immune resistance always occurs due to the enhanced programmed cell death-ligand 1 (PD-L1) expression after PTX@Alb treatment, which then leads to immune tolerance. To fill these gaps, we newly revealed that tamoxifen (TAM), a clinically widely used adjuvant therapy for breast cancer with mitochondrial metabolism blockade capacity, could also be used as a novel effective PD-L1 and TGF-β dual-inhibitor *via* inducing the phosphorylation of adenosine 5'-monophosphate-activated protein kinase (AMPK) protein. Following this, to obtain a more significant effect, TPP-TAM was prepared by conjugating mitochondria-targeted triphenylphosphine (TPP) with TAM, which then further self-assembled with albumin (Alb) to form TPP-TAM@Alb nanoparticles. By doing this, TPP-TAM@Alb nanoparticles effectively decreased the expression of collagen *in vitro*, which then led to the enhanced accumulation of PTX@Alb in 4T1 tumors. Besides, TPP-TAM@Alb also effectively decreased the expression of PD-L1

*Corresponding authors.
E-mail addresses: dh0726@163.com (Hui Deng), sjl1@wmu.edu.cn, shenjl@wiucas.ac.cn (Jianliang Shen).
[†]These authors made equal contributions to this work.
Peer review under the responsibility of Chinese Pharmaceutical Association and Institute of Materia Medica, Chinese Academy of Medical Sciences.

https://doi.org/10.1016/j.apsb.2024.05.028

and TGF-β in tumors to better sensitize PTX@Alb-mediated chemo-immunotherapy by enhancing T cell infiltration. All in all, we newly put forward a novel mitochondrial metabolism blockade strategy to inhibit PTX@Alb-resistant tumors, further supporting its better clinical application.

1. Introduction

Recently, female breast cancer became the most commonly diagnosed cancer, with an estimated 2.3 million new cases worldwide (11.7% of all the cases), followed by lung (11.4%), colorectal (10.0%), prostate (7.3%), and stomach (5.6%) cancers[1,2]. Due to such a serious situation, chemotherapy was developed as the universal strategy to cure breast tumors, among which FDA-approved albumin-bound paclitaxel nano-formulation (named PTX@Alb in this study) was widely used[3,4]. Apart from working as an anti-tubulin drug to induce tumor cell apoptosis, PTX@Alb also could reverse the immune-resistance microenvironment by inducing immunogenic cell death (ICD) and enhancing T cell infiltration to generate the antigen-specific immune response[5,6]. Even so, only mild therapeutic outcomes were achieved due to the limited PTX@Alb accumulation in tumors at least partly induced by transforming growth factor (TGF-β)-caused dense collagen distribution[7–9]. Apart from this, after PTX@Alb treatment, the expression of PD-L1 was always enhanced to some extent by promoting STAT1 phosphorylation, which then may also lead to chemo-immunotherapy resistance[10–13]. Therefore, the efficacy of PTX@Alb in treating tumors, especially breast cancer, is still limited and needs to be improved.

For the past few years, mitochondrial metabolism blockage had aroused great interest owing to its unexpected capacity in reversing immune resistance induced by increased levels of oxidative phosphorylation (OXPHOS) and glycolysis in tumors[14–17]. When mitochondrial metabolism was depressed by OXPHOS or glycolysis inhibition, the adenosine diphosphate (ADP)/adenosine triphosphate (ATP) ratio was raised, resulting in the following enhanced phosphorylation levels of AMPK protein[14,18–20]. Following this, the endoplasmic reticulum (ER)-associated degradation of the PD-L1 protein was then enhanced, leading to the finally decreased tumor cell membrane location of PD-L1[14,18,19,21,22]. In addition, due to increased phosphorylation levels of AMPK protein, the secretion of TGF-β and collagen from tumor cells could also be remised[23–26]. Apart from limiting drug accumulation in tumors, TGF-β and collagen both were newly proven to work as immune suppression proteins *via* limiting T cell infiltration and impairing the tumor cell-killing efficacy of T cells, as well as recruiting amounts of regulatory T cells[23,27–29]. Thus, mitochondrial metabolism blockage by OXPHOS or glycolysis inhibition may serve as a versatile strategy to sensitize PTX@Alb-mediated chemo-immunotherapy *via* reversing the immune-resistance tumor microenvironment and enhancing PTX@Alb distribution in tumors. But, whether this strategy could work as predicted has yet to be confirmed since little attention noticed the potential of such a strategy[30–32].

At present, TAM is widely used as an adjuvant chemotherapy drug for estrogen receptor-positive breast cancer, which effectively extends the survival time and life quality of some breast cancer patients to some extent[30,33,34]. Interestingly enough, apart from working as an anti-estrogen drug, it was also revealed that TAM could also depress OXPHOS *via* inhibiting mitochondrial complex I in the electron transport chain[30,31,35]. Due to this, the AMPK pathway was activated due to the raised ADP/ATP ratio, meaning that TAM may possess the capacity to inhibit PD-L1, collagen, and TGF-β immune pathway, simultaneously[14,23,36]. But, whether TAM possesses such capacity to inhibit collagen, TGF-β, and PD-L1 expression through affecting the AMPK pathway as we predicted still needs to be proved[37]. Apart from this, as an adjuvant chemotherapeutic drug, TAM possessed no tumor-targeting capacity, which may limit the accumulation of TAM in tumors, as well as induce side effects and acquired resistance of TAM[31,38]. Thus, targeted delivery of TAM to the tumors may serve as a novel strategy to better convert cold tumors to hot ones after PTX@Alb-based chemotherapy *via* reversing immune-resistance tumor microenvironment and enhancing PTX@Alb distribution.

As we all know, cationic TPP possesses ideal tumor mitochondria targeting capacity[39,40]. Interestingly enough, it was also newly revealed that conjugating TAM with mitochondria-targeting agents may decrease the dosage of TAM needed to induce mitochondria metabolism blockage[31]. Thus, we believed that conjugating TAM with TPP may be used as a novel strategy to better sensitize PTX@Alb-based chemo-immunotherapy by PD-L1 and TGF-β co-depression (Scheme 1). To prove this speculation, TPP-TAM was designed and prepared by conjugating mitochondria-targeted TPP with mitochondrial complexes I depression agent TAM, which was then proved to possess PD-L1 and TGF-β co-depression capacity at a relatively lower dosage as desired (TAM 20 μmol/L *vs* TPP-TAM 1 μmol/L). Following this, TPP-TAM was further self-assembled with Alb to form TPP-TAM@Alb nanoparticles to better deliver it to 4T1 tumors by using the previously reported method (Scheme 1)[41]. By doing this, TPP-TAM@Alb nanoparticles depressed TGF-β expression and inhibited collagen secretion, leading to the following enhanced accumulation of Chlorin e6 (Ce6) co-loaded PTX@Alb in 4T1 tumors. Apart from this, TPP-TAM@Alb then sensitized tumor chemo-immunotherapy by amplifying T cell infiltration due to the prevented possible acquired immune resistance induced by PTX@Alb through PD-L1 and TGF-β co-depression. To sum up, in this study, we innovatively designed a mitochondrial metabolism blockade strategy by using TPP-TAM@Alb nanoparticles to sensitize chemotherapy-resistant tumors.

2. Materials and methods

2.1. Materials

Rabbit anti-mouse AMPK antibody (#2532L), rabbit anti-mouse TGF-β antibody (#3711S), rabbit anti-mouse pAMPK (Thr172) antibody (#2535L), and rabbit anti-mouse collagen I antibody (#72026S) were all obtained from Cell Signaling Technology

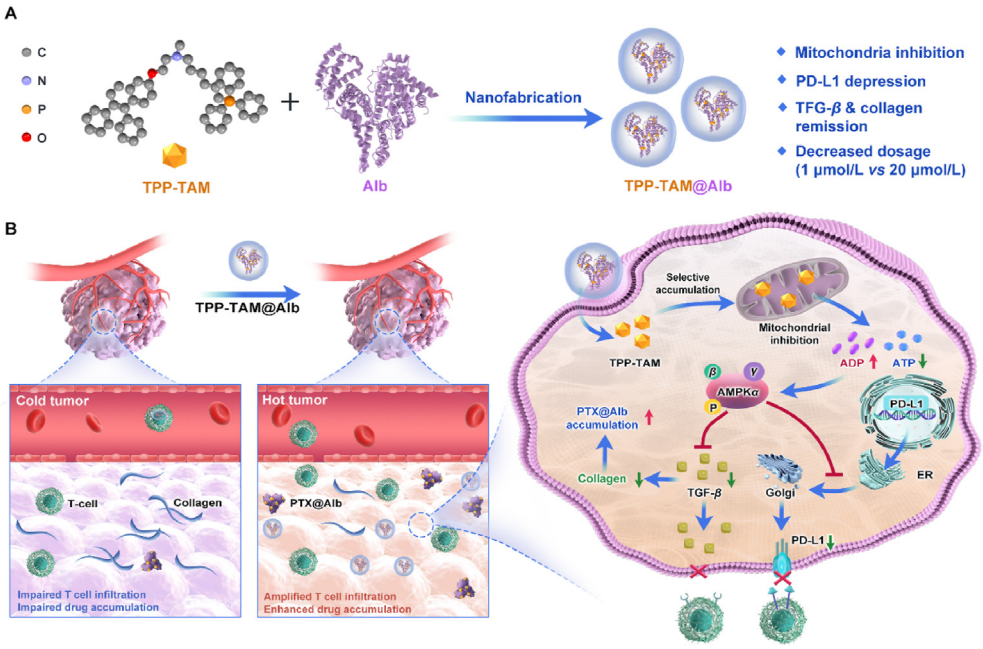

Scheme 1 (A) The preparation process of TPP-TAM@Alb. (B) The mechanism underlying TPP-TAM@Alb boosted PTX@Alb-based chemo-immunotherapy *via* mitochondrial metabolism blockade-induced enhanced drug accumulation and amplified T-cell infiltration.

(Boston, MA, USA). Rabbit anti-mouse PD-L1 antibody (#DF6526), rabbit anti-mouse β-actin antibody (#AF7018), Affinity™ Enhanced Chemiluminescence (ECL) kit (#KF8001), rabbit anti-mouse HIF-1α antibody (#AF1009), goat anti-Rabbit IgG (H+L) Horse Radish Peroxidase (HRP) antibody (#S0001), rabbit anti-mouse Ki67 antibody (#AF0198), rabbit anti-mouse high mobility group protein 1 (HMGB1) antibody (#AF7020), rabbit anti-mouse Bcl-2 antibody (#AF6139), and rabbit anti-mouse Calreticulin (CRT) antibody (#DF3139) were purchased from Affinity Biosciences LTD (Cincinnati, OH, USA). Serum Alb was obtained from Sigma Chemical Co., Ltd. (Darmstadt, Germany). Trypsin-Ethylenediaminetetraacetic acid disodium salt, Dulbecco's modified Eagle medium (DMEM), penicillin/streptomycin, and fetal bovine serum (FBS) were purchased from GIBCO-BRL (Grand Island, NY, USA). FITC-labeled rat anti-mouse CD3 antibodies (#100204), APC-labeled rat anti-mouse CD8 antibodies (#100712), and PE-labeled rat anti-mouse CD4 antibodies (#100408) were obtained from Biolegend (San Diego, CA, USA). Dorsomorphin (Com C), Chlorin e6 (Ce6), 1,6-dibromohexane, TAM, dimethylformamide (DMF), triphenylphosphine (TPP), DMSO-d_6, hexyltriphenylphosphonium bromide (TPP-C6), methanol, 2-mercaptoethanol, and dichloromethane were provided by Aladdin (Shanghai, China). InVivoMAb anti-mouse PD-L1 (#BE0101) was obtained from Bio X Cell (Lebanon, NH, USA). All the materials or chemicals used in the Western blot assay including RIPA lysis buffer, primary antibody diluent, second antibody diluent, skim milk powder, etc., were bought from Beyotime Biotechnology (Shanghai, China). PTX@Alb was obtained from Abraxis BioScience (Los Angeles, CA, USA). Alanine transaminase (ALT) detection kit (#C009-2-1), urea nitrogen (BUN) detection kit (#C013-2-1), serum creatinine (CRE) detection kit (#C011-2-1), and aspartate transaminase (AST) (#C010-2-1) detection kit by the relevant assay kits obtained from Jiancheng Bioengineering Institute (Nanjing, China). All antibodies or materials used in Western blot assay, flow cytometry, etc., were all based on the manufacturer's instructions. Unless otherwise noted, all chemicals, antibodies, and other materials were used directly without further purification.

2.2. *Cell culture and animals*

Murine breast tumor 4T1 cells were cultured in DMEM containing 10% FBS and 1% penicillin/streptomycin and then incubated at 37 °C in a 5% CO_2 humidified atmosphere (Thermal Fisher Inc., Waltham, MA, USA).

BALB/c female mice (6−8 weeks, 18−20 g) were purchased from the Experiment Animal Center of Wenzhou Medical University (Zhejiang, China). All animal experiments were performed following the Experimental Animal Administration Committee of Zhejiang Province and the ethical guidelines for animal experiments of Wenzhou Medical University (xmsq2022-1020).

2.3. *Synthetic process of TPP-TAM*

Generally, TAM-NH (Supporting Information Fig. S1) was prepared as previously reported[31,42]. Synthesis of TAM-C6 (Fig. S1): TPP-C6 was obtained by the reaction between 1.46 g 1,6-dibromohexane and 1.07 g TAM-NH in 140 mL DMF. The solution was stirred at 85 °C for 24 h. Following this, the reaction mixture was rotor-evaporated to collect the crude solid of TAM-C6. Then, the silica gel column chromatography was used to obtain the desired TAM-C6 (512 mg, yield about 33.0%, ∼95% pure) by utilizing methanol and dichloromethane as the developing solvent.

Synthesis of TPP-TAM (Fig. S1): TPP-TAM was obtained by the reaction between 260.3 mg TAM-C6 and 262.3 mg TPP in 50 mL DMF. The solution was stirred at 85 °C for 24 h. Following this, the reaction mixture was rotor-evaporated to collect the crude solid of TPP-TAM. Then, the silica gel column chromatography was used to obtain the desired TPP-TAM (105 mg, yield about 26.8%, ∼95% pure) by utilizing methanol and dichloromethane as the developing solvent. Then, ^{1}H nuclear magnetic resonance (^{1}H NMR, QOne Instruments, QUANTUM-I-400MHz, Wuhan, China)

was used to confirm the right preparation of TPP-TAM and TAM-C6 by using DMSO-d_6 as the solvent, which was further confirmed by high-resolution mass spectrum (HR-MS) (ESI-TOF) (detection for TPP-TAM: $[M]^+ = 702.3832$, $[M+H]^{2+} = 351.6937$).

2.4. Preparation and characterization of TPP-TAM@Alb

TPP-TAM@Alb was prepared by referring to the previously reported method[34,43]. Generally, 200 mg of Alb was dissolved in 100 mL of deionized water with constant stirring. Then, 2-mercaptoethanol was added to expose the hydrophobic region of Alb, after which 0.5 mL TPP-TAM (10 mg/mL, dissolved in ethanol) was slowly added into the denatured protein solution to obtain the light blue TPP-TAM@Alb solution. Following this, free 2-mercaptoethanol and free TPP-TAM were removed using an ultrafiltration membrane (cut-off weight: 30 kDa) (Merck, Millipore 8400, Darmstadt, Germany). Finally, TPP-TAM@Alb nanoparticles were stored at 4 °C for further usage.

The morphology of TPP-TAM@Alb nanoparticles was characterized with a negative stain method (1% phosphotungstic acid) using transmission electron microscopy (TEM) (Thermo Fisher Scientific, FEI Talos F200S, Waltham, MA, USA). The distribution of the particle size and zeta potential of nanoparticles were observed with a Zetasizer (Malvern, Zetasizer Nano ZS ZEN3600, Malvern, UK). To observe the physiological stabilities of TPP-TAM@Alb, Zetasizer was used to dynamically monitor their hydrated diameters after being incubated in PBS and ultrapure water for varying time intervals over 48 h at room temperature environment to observe the particle size changes. The drug loading efficiency (LE) and drug encapsulation efficiency (EE) of TPP-TAM were determined by UV−Vis spectrometer (PerkinElmer, Lambda 25, Waltham, MA, USA) after Alb precipitation with excess dichloromethane as in Eqs. (1) and (2):

$$\text{LE (\%)} = (\text{Weight of TPP-TAM in TPP-TAM@Alb/Total weight of TPP-TAM@Alb}) \times 100 \quad (1)$$

$$\text{EE (\%)} = (\text{Weight of TPP-TAM in TPP-TAM@Alb/Total weight of TPP-TAM fed initially}) \times 100 \quad (2)$$

The release profile of TPP-TAM@Alb was detected as the previously reported similar method[44]. Generally, TPP-TAM@Alb was sealed in the dialysis bag (molecular weight cutoff, 3.5 kDa), immersed in 500 mL PBS buffer containing 2% β-cyclodextrin, and shaken at 200 rpm at room temperature. 1 mL osmotic fluid was collected from the PBS buffer and the same volume of PBS was added at different times. At last, TPP-TAM concentration in the osmotic fluid was quantified by UV−Vis spectrometer.

2.5. In vitro cytotoxicity

7×10^3 4T1 cells were cultured in 96-well plates with DMEM medium containing different concentrations of TPP-TAM@Alb, PTX@Alb, or TPP-TAM@Alb + PTX@Alb for 24 h. Then, the CCK-8 assay was added to each well. After incubation at 37 °C for another 2 h, the absorbance at 450 nm was measured using a plate reader (BioTek, Epoch 2, Santa Clara, CA, USA).

2.6. Cell apoptosis analysis

Cell apoptosis detection was used as an important index to evaluate the cytotoxicity of PTX@Alb and TPP-TAM@Alb. Generally, 10^5 4T1 cells were added and cultured in 6-well plates. After 24 h, cells were incubated with TPP-TAM@Alb, PTX@Alb, TPP-TAM@Alb + PTX@Alb (TPP-TAM concentration: 1 μmol/L, PTX concentration: 10 μmol/L) for another 8 h. Then, 4T1 cells were collected by trypsinization and low-speed centrifugation, washed by PBS, and co-stained with Annexin V-FITC and Propidium Iodide (PI) for 30 min before the final flow cytometry analysis. Similarly, the cell apoptosis was also detected by using Calcein-AM when 4T1 cells were incubated with TPP-TAM@Alb, PTX@Alb, or TPP-TAM@Alb + PTX@Alb (TPP-TAM concentration: 1 μmol/L, PTX concentration: 10 μmol/L).

2.7. Cell clone assay

To observe the effect of nanoparticles on tumor inhibition over a longer period, the cell clonal formation experiment was conducted. 1×10^3 4T1 cells of all groups were seeded in 6-well plates after being treated with TPP-TAM@Alb, PTX@Alb, TPP-TAM@Alb + PTX@Alb (TPP-TAM concentration: 1 μmol/L, PTX concentration: 10 μmol/L), and no-processing group, respectively. After incubation for 14 days, 4T1 macroscopic cell colonies were formed and stained by crystal violet.

2.8. Mitochondrial complexes activity assay

To confirm the effects of different concentrations of TAM and TPP-TAM on mitochondrial complexes function, MitoCheck Complex I Activity Assay Kit (Cayman Chemical, #700930, Ann Arbor, MI, USA) was used according to the manufacturer's instruction.

2.9. Detection of mitochondrion membrane potential by JC-1 probe

JC-1 mitochondrial membrane potential probe (Beyotime Biotechnology, Shanghai, China) was used for the detection of mitochondrial depolarization. Generally, 5×10^4 4T1 cells were seeded in glass-bottom cell culture dishes (Nest Biotechnology Co., Ltd., Wuxi, China). 24 h later, the cells were treated with PBS, 20 μmol/L TPP-C6, 20 μmol/L TAM, or 2 μmol/L TPP-TAM for another 24 h. Carbonyl cyanide 3-chlorophenylhydrazone (10 μmol/L CCCP) was treated as the positive control. Subsequently, the cells were labeled with 5 μg/mL JC-1 reagents for another 20 min at 37 °C. At last, the monomer fluorescence signals of JC-1 (green) were observed by using confocal laser scanning microscopy (Nikon, CLSM A1, Tokyo, Japan).

2.10. Western blot assay

Western blotting analysis was conducted as previously reported[39]. RIPA buffer (Beyotime, Shanghai, China) was used for the extraction of proteins from the tumor cells or tissues. The protein concentration of each sample was determined by Bicinchoninic Acid (BCA) kits (Beyotime, Shanghai, China). Proteins were separated by 10% SDS-PAGE and then transferred to a 0.45 μm Polyvinylidene Fluoride (PVDF) membrane (Merck, #IPVH00010, Darmstadt, Germany). The membrane was blocked with 5% skimmed milk at room temperature for 1 h and incubated with relevant primary antibodies to TGF-β (1:1000, CST, MA, USA), PD-L1 (1:1000, Affinity Biosciences Inc., OH, USA), AMPK (1:1000, CST, MA, USA), pAMPK (1:1000, CST, MA,

USA), collagen I (1:1000, CST, MA, USA), Bcl-2 (1:1000, Affinity Biosciences Inc., OH, USA), or β-actin (1:5000, Affinity Biosciences Inc., OH, USA) at 4 °C overnight. After washing with TBST buffer, the PVDF membrane was then incubated with goat anti-rabbit IgG (H + L) HRP antibody (dilution factor 1:5000, Affinity Biosciences Inc., OH, USA) at room temperature for 1 h. After washing with TBST buffer (mixture of tris-buffered saline and tween 20) repeatedly to wipe off the unbound secondary antibodies, the images of protein bands were visualized by using a fluorescent & chemiluminescence gel-imaging system (Peiqing Science and Technology Co., Ltd., JS-M6P, Shanghai, China). All the standardized protein expression levels were finally quantified by ImageJ.

2.11. Determination of ADP and ATP content

7×10^3 4T1 cells were seeded in the 96-well plates overnight and then incubated with 2 μmol/L TPP-TAM for different time. At 1, 3, 6, 12, and 24 h after TPP-TAM treatments, 4T1 cells were collected and lysed for the detection of ATP and ADP content by using the ADP/ATP detection kit (Vigorous Biotechnology Co., Ltd., #T008, Beijing, China).

2.12. Evaluation of ICD generation in vitro

To evaluate the influence of TPP-TAM@Alb on the efficacy of PTX@Alb in inducing tumor ICD, the immunofluorescence staining of CRT and HMGB1 was conducted. Generally, 5×10^4 4T1 cells were first seeded in glass-bottom cell culture dishes. 24 h later, 4T1 cells were treated with PBS, TPP-TAM@Alb, PTX@Alb, and TPP-TAM@Alb + PTX@Alb (concentration of TPP-TAM: 1 μmol/L, concentration of PTX: 10 μmol/L). After another 12 h, 4T1 cells were fixed with 4% paraformaldehyde for 15 min at room temperature followed by PBS washing three times. Then, the cells were sequentially stained with anti-CRT primary antibodies (1: 500, Affinity, OH, USA) and anti-HMGB1 primary antibodies (1:500, Affinity, OH, USA) at 4 °C overnight. Subsequently, cells were stained with Alexa Fluor 594 labeled goat anti-rabbit IgG (H+L) (1: 2500, Thermo Scientific, MA, USA). Finally, DAPI was used to stain the cell nucleus for 10 min. The immunofluorescence signals of CRT and HMGB1 were finally observed by confocal laser scanning microscopy.

2.13. Effects of TPP-TAM@Alb on the bio-distribution of Ce6@Alb or PTX@Alb in vivo

In this study, Ce6 with near-infrared fluorescence was used as an indicator to evaluate the effects of TPP-TAM@Alb on the bio-distribution of PTX@Alb *in vivo*. Firstly, Ce6 co-loaded PTX@Alb nanosystem (named Ce6@PTX@Alb) was prepared using the similar methods described previously[41,43,44].

Female BALB/c mice were injected subcutaneously with 1×10^6 4T1 cells under the right axilla. When the volume of tumors reached around 150 mm^3, the mice were divided into two groups randomly ($n = 3$). TPP-TAM@Alb (TPP-TAM concentration: 5 mg/kg) and the corresponding 0.9% saline (as a control group) were first intravenously injected by the tail, respectively. After 24 h, mice were intravenously injected with 0.6 mg/kg Ce6@PTX@Alb (Ce6 concentration: 0.6 mg/kg; PTX concentration: 5 mg/kg). Following this, the mice were sacrificed to collect the tumors and major tissues (heart, liver, spleen, lung, and kidney) for *ex vivo* NIR fluorescence imaging at different time (12, 24, 48, and 72 h). The images of fluorescence distribution in mice were acquired and evaluated by the multi-mode optical live imaging system (PerkinElmer, IVIS Lumina XRMS Series III, Waltham, MA, USA).

Female BALB/c mice were injected subcutaneously with 1×10^6 4T1 cells in the breast fat pad that near the right abdomen. When the volume of tumors reached around 100 mm^3, the mice were divided into two groups randomly ($n = 5$). TPP-TAM@Alb (TPP-TAM concentration: 5 mg/kg) and the corresponding 0.9% saline (as a control group) were first intravenously injected by the tail, respectively. After 24 h, mice were intravenously injected with 5 mg/kg PTX@Alb (PTX concentration: 5 mg/kg). After another 24 h, all the mice were sacrificed to collect the tumors and then used to detect the accumulation of PTX in 4T1 tumors by HPLC[7].

2.14. Analysis of T cells infiltration in vivo

The effects of different treatments on the infiltration of T cells in tumors were observed by using the subcutaneously implanted 4T1 tumor-bearing mice. First, BALB/c mice were injected subcutaneously with 1×10^6 4T1 cells under the right axilla. When the volume of tumors reached around 100 mm^3, the mice were divided into six groups randomly ($n = 5$): 1. Vehicle; 2. PTX@Alb; 3. TPP-TAM@Alb; 4. PTX@Alb + TPP-TAM@Alb; 5. Anti-PD-L1 antibodies; 6. PTX@Alb + Anti-PD-L1 antibodies (calculated by TPP-TAM concentration: 5 mg/kg; PTX concentration: 5 mg/kg; anti-PD-L1 antibody concentration: 5 mg/kg). The mice were firstly treated with TPP-TAM@Alb nanoparticles or anti-PD-L1 antibodies by tail vein injection, followed by PTX@Alb treatment in the same way at 24 h later. After another 24 h, the tumors were collected to evaluate the immune cell infiltration in tumors. Part of the tumors was enzymatically degraded as previously reported[45,46]. Then, the cells obtained from tumors were collected to detect the $CD3^+$, $CD4^+$, and $CD8^+$ T cells by flow cytometry assay (Beckman Coulter, CytoFLEX, Brea, CA, USA) by using FITC-labeled CD3 antibodies, APC-labeled CD8 antibodies, and PE-labeled CD4 antibodies.

The effects of different treatments on the infiltration of T cells in tumors were also observed by using breast fat pad implanted 4T1 tumor-bearing mice. First, BALB/c mice were injected subcutaneously with 1×10^6 4T1 cells in the breast fat pad near the right abdomen. When the volume of tumors reached around 100 mm^3, the mice were divided into six groups randomly ($n = 5$): 1. Vehicle; 2. PTX@Alb; 3. TPP-TAM@Alb; 4. PTX@Alb + TPP-TAM@Alb (calculated by TPP-TAM or PTX concentration: 5 mg/kg). The mice were firstly treated with TPP-TAM@Alb nanoparticles by tail vein injection, followed by PTX@Alb treatment at 24 h later in the same way. After another 24 h, the tumors were collected to evaluate the immune cell infiltration in tumors. Part of the tumors was enzymatically degraded as previously reported[45,46]. Then, the cells obtained from tumors were collected to detect the $CD3^+$, $CD4^+$, and $CD8^+$ T cells by flow cytometry assay.

2.15. Evaluation of tumor apoptosis and proliferation in vivo

Female BALB/c mice were subcutaneously injected with 1×10^6 4T1 cells under the right axilla. When the volume of tumors reached around 100 mm^3, these mice were randomly divided into the following six groups ($n = 3$): 1. Vehicle; 2. PTX@Alb; 3. TPP-TAM@Alb; 4. PTX@Alb + TPP-TAM@Alb; 5. Anti-PD-L1 antibodies (calculated by TPP-TAM concentration:

5 mg/kg; PTX concentration: 5 mg/kg; anti-PDL1 concentration: 5 mg/kg). The mice were firstly treated with TPP-TAM@Alb nanoparticles by tail vein injection, followed by PTX@Alb treatment 24 h later in the same way. After another 24 h, to evaluate the tumor cell apoptosis and proliferation in the 4T1 tumors, all the mice were sacrificed to collect 4T1 tumors for the immunofluorescence analysis of Ki67, TUNEL, and hematoxylin−eosin (H&E) staining for histological analysis. Briefly, the tumors of different groups were collected and embedded in OCT and cut into 7 μm slices. Next, a one-step TUNEL assay kit (Beyotime, Shanghai, China) was used to stain tumor tissue slices, and tumor apoptosis was analyzed by CLSM. Meanwhile, for Ki67-based cell proliferation ability assessment, the samples were fixed and incubated overnight with rabbit anti-mouse Ki67 antibody (dilution factor 1:1000, Affinity Biosciences Inc., OH, USA) and then incubated with Alexa Fluor 594-labeled goat anti-rabbit IgG (H+L) (dilution factor 1:1000, Thermo Scientific, MA, USA) at room temperature for 1 h. The last step was the detection of the fluorescence images by CLSM. ImageJ was used to calculate the mean fluorescence intensity (MFI) of TUNEL and Ki67.

2.16. Evaluation of the combination anti-tumor efficacy of TPP-TAM@Alb and PTX@Alb in subcutaneously implanted 4T1 tumors

Female BALB/c mice were subcutaneously injected with 1×10^6 4T1 cells under the right axilla. When the volume of tumors reached around 100 mm^3, these mice were randomly divided into the following six groups ($n = 5$): 1. Vehicle; 2. PTX@Alb; 3. TPP-TAM@Alb; 4. PTX@Alb + TPP-TAM@Alb; 5. Anti-PD-L1 antibodies; 6. PTX@Alb + Anti-PD-L1 antibodies (calculated by TPP-TAM concentration: 5 mg/kg; PTX concentration: 5 mg/kg; anti-PD-L1 concentration: 5 mg/kg). The mice were firstly treated with TPP-TAM@Alb nanoparticles or anti-PD-L1 antibodies by tail vein injection, followed by PTX@Alb treatment at 24 h later.

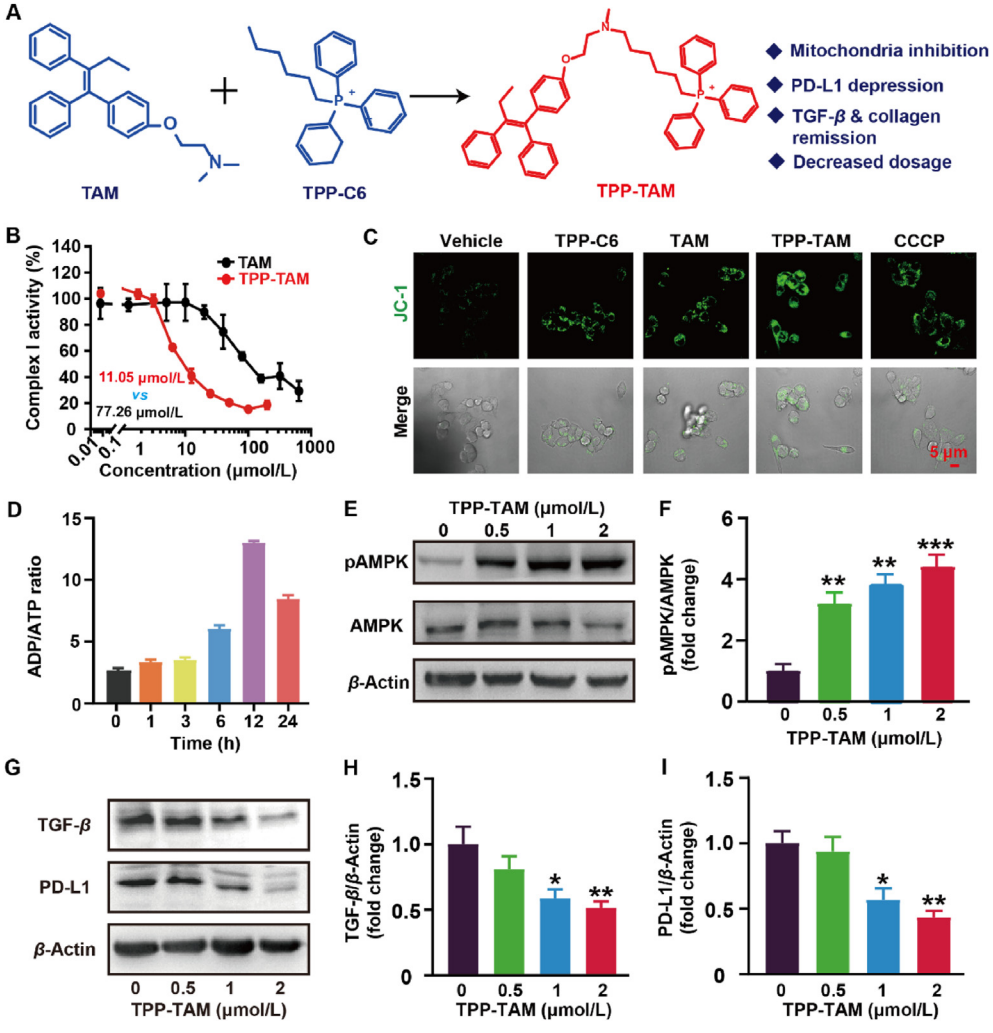

Figure 1 Effects of TPP-TAM on the expression of PD-L1 and TGF-β protein in 4T1 lung tumor cells. (A) The preparation process of TPP-TAM and its merits compared with TAM. (B) Evaluation of the effects of different concentrations of TAM or TPP-TAM on the function of mitochondrial complex I ($n = 3$). (C) Detection of the changes of mitochondrial membrane potential by JC-1 fluorescence (monomer, green) after PBS, 20 μmol/L TPP-C6, 20 μmol/L TAM, 2 μmol/L TPP-TAM, or 10 μmol/L CCCP treatment, scale bar = 5 μm. (D) Detection of the ADP/ATP ratio at different time after 2 μmol/L TPP-TAM treatment ($n = 3$). (E−I) Evaluation and quantification of the expression levels of PD-L1, AMPK, pAMPK, and TGF-β proteins by Western blot assay ($n = 3$). All data are presented as mean ± SD. $^*P < 0.05$, $^{**}P < 0.01$, and $^{***}P < 0.001$.

The tumor length, tumor width, and body weight were measured every two days to observe the growth of tumors, whose volumes were calculated using Eq. (3):

$$V = L/2 \times W^2 \quad (3)$$

where L means longer dimension and W means shorter dimension). 14 days later, mice were executed to collect the 4T1 tumors, which then were weighed to assess tumor size.

2.17. *Evaluation of the combination anti-tumor efficacy of TPP-TAM@Alb and PTX@Alb in breast fat pad implanted 4T1 tumors*

Female BALB/c mice were subcutaneously injected with 1×10^6 4T1 cells under the breast fat pad that near the right abdomen. When the volume of tumors reached around 50 mm^3, these mice were randomly divided into the following six groups ($n = 6$): 1. Vehicle; 2. TAM; 3. PTX; 4. PTX@Alb; 5. TPP-TAM@Alb; 6. PTX@Alb + TPP-TAM@Alb (calculated by PTX, TAM, or TPP-TAM concentration: 5 mg/kg). The mice were firstly treated with TPP-TAM@Alb nanoparticles by tail vein injection, followed by PTX@Alb treatment at 24 h later. The tumor length, tumor width, and body weight were measured every two days to observe the growth of tumors, whose volumes were calculated using Eq. (3). 14 days later, mice were executed to collect the 4T1 tumors, which then were weighed to assess tumor size.

2.18. *Biosafety evaluation of TPP-TAM@Alb*

The healthy BABL/c mice were intravenously injected with TPP-TAM@Alb (TPP-TAM concentration: 5 mg/kg) or the equal volume Vehicle (0.9% normal saline). After 48 h, mice were sacrificed to collect the major organs including the heart, lung, spleen, liver, and kidney, which then were fixed with 4% paraformaldehyde and embedded in paraffin for further H&E staining. Apart from this, blood was also acquired from BABL/c mice and

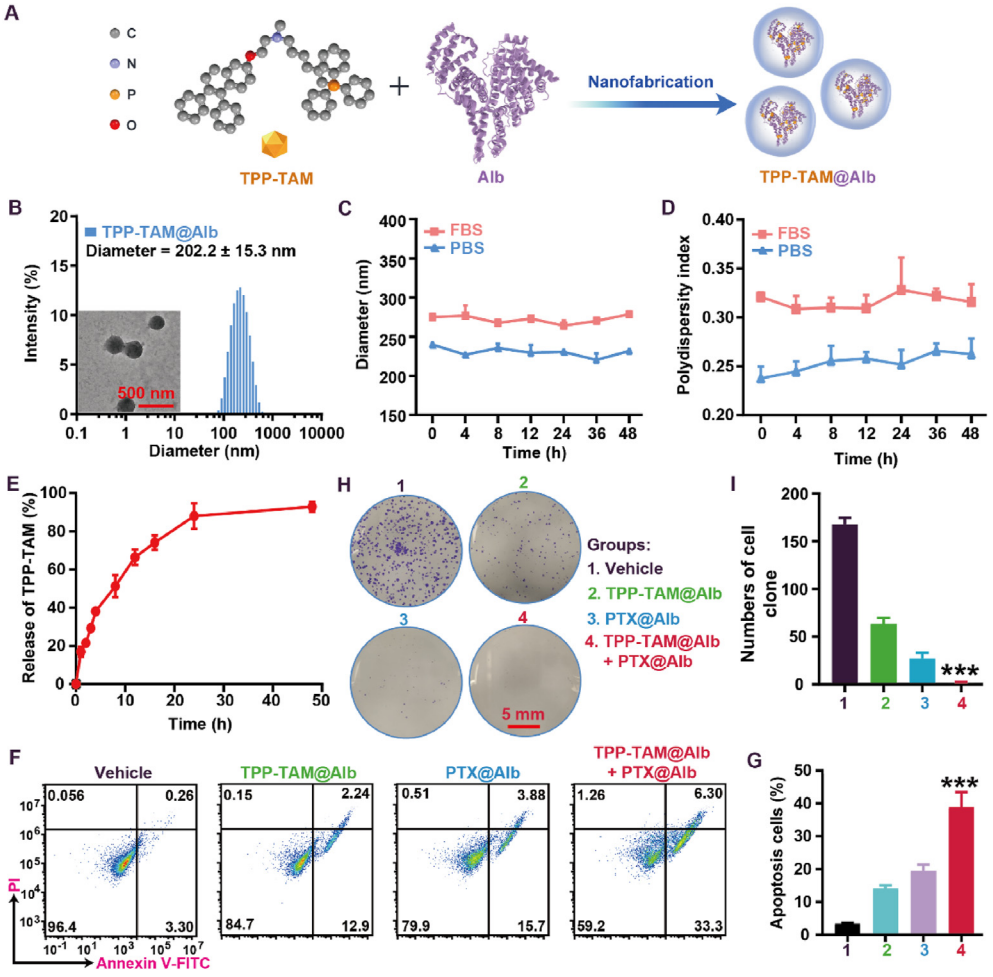

Figure 2 Preparation of TPP-TAM@Alb nanoparticles and evaluation of its ability in promoting the tumor-killing capacity of PTX@Alb *in vitro*. (A) The preparation process of TPP-TAM@Alb. (B) The diameters and morphology of the prepared TPP-TAM@Alb, scale bar = 500 nm. (C, D) Evaluation of the stability of TPP-TAM@Alb in PBS or 5% FBS buffer ($n = 3$). (E) The drug release behavior of the encapsulated TPP-TAM@Alb in TPP-TAM@Alb nanoparticles ($n = 3$). (F, G) The combination therapy efficacy of PTX@Alb and TPP-TAM@Alb in inducing tumor cell apoptosis evaluated by the Annexin V-FITC and PI stained cells through using flow cytometry assay ($n = 3$). (H) The typical images of 4T1 cell clones after different treatments, scale bar = 5 mm. (I) Quantification of the numbers of 4T1 cell clones after different treatments ($n = 3$). All data are presented as mean ± SD. ***$P < 0.001$.

then centrifuged at 2000 rpm (Thermal Fisher Inc., Fresco™ 21, Waltham, MA, USA) for 5 min at 4 °C to take the supernatant serum. To evaluate the influence of TPP-TAM@Alb on the function of the liver and spleen, serum was used to detect the expression levels of ALT, BUN, CRE, and AST by the relevant assay kits obtained from the Jiancheng Bioengineering Institute. Moreover, the long-term bio-safety of TPP-TAM@Alb (TPP-TAM concentration: 5 mg/kg) or the equal volume Vehicle (0.9% normal saline) was also evaluated by using the healthy BABL/c mice (twice a week). After 14 days, mice were sacrificed to collect the major organs including the heart, lung, spleen, liver, and kidney, which then were fixed with 4% paraformaldehyde and embedded in paraffin for H&E staining.

2.19. *Hemolysis assay*

The blood was obtained from BABL/c female mice and then centrifuged at 2000 rpm for 4 min to acquire the red blood cells (RBCs). Next, RBCs were added to TPP-TAM@Alb (100 μL) at different concentrations (TPP-TAM concentration: 0, 0.01, 0.1, 1, or 10 mg/mL) to determine the hemolysis activity of TPP-TAM@Alb. Meanwhile, PBS buffer and water were used as the negative control and the positive control, respectively. After incubating at 37 °C for 2 h, all the samples were centrifuged to obtain the supernatants. At last, the UV absorption of the supernatants at 541 nm was recorded to calculate the corresponding hemolysis ratios.

2.20. *Statistical analysis*

Data were shown as the mean ± standard deviation (SD). Statistical analysis was performed *via* a two-tailed Student's *t*-test for the comparison of two groups or one-way ANOVA test for the comparison of multiple groups. Besides, *post hoc* analysis was performed using the Wilcoxon rank-sum test with a Bonferroni correction when needed. $^{*}P < 0.05$ was considered statistically significant. $^{**}P < 0.01$ and $^{***}P < 0.001$ were extremely significant. ns, no significant difference, $P > 0.05$.

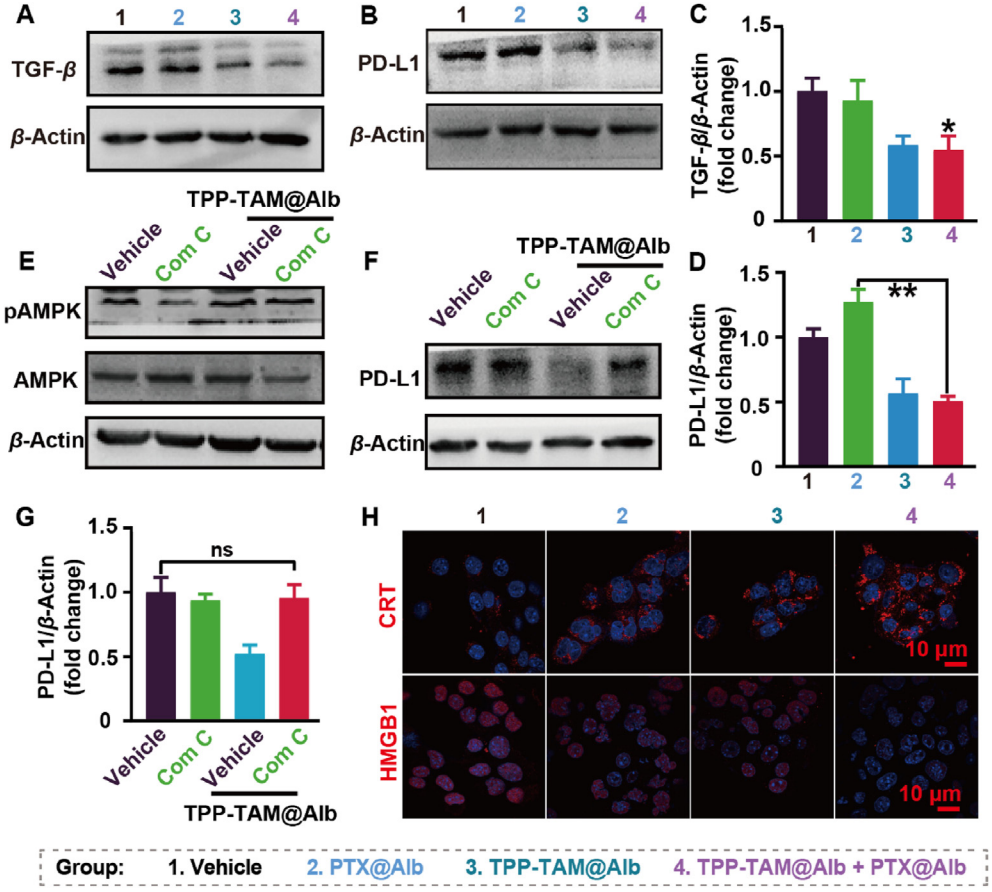

Figure 3 Effects of TPP-TAM@Alb on the expression of PD-L1 and TGF-β proteins in 4T1 cells. (A, B) The typical image of PD-L1 and TGF-β proteins detected by Western blot assay after different treatments. (C, D) Quantification of the expression levels of PD-L1 and TGF-β proteins after various treatments ($n = 3$). (E) The typical image of AMPK and pAMPK proteins detected by Western blot assay after TPP-TAM@Alb treatment in the presence or absence of Com C (used as AMPK inhibitor to depress AMPK pathway). (F, G) Evaluation and quantification of the expression levels of PD-L1 proteins by Western blot assay after TPP-TAM@Alb treatment in the presence or absence of Com C ($n = 3$). (H) The representative immunofluorescence images of CRT and HMGB1 after PTX@Alb, TPP-TAM@Alb, or PTX@Alb and TPP-TAM@Alb combination therapy, scale bar = 10 μm. All data are presented as mean ± SD. $^{*}P < 0.05$, $^{**}P < 0.01$. ns, not significant, $P > 0.05$.

3. Results and discussion

3.1. TPP-TAM inhibited PD-L1 and TGF-β expression in 4T1 cells

For the past few years, TAM has been widely used as adjuvant therapy for the endocrine treatment of a variety of breast cancers[30,31]. Apart from this, it was also revealed that TAM could inhibit OXPHOS by affecting the mitochondrial complex I function, which then led to the enhanced phosphorylation of AMPK protein by raising the ADP/ATP ratio[30,47]. Due to this, considering the vital role of the AMPK pathway in regulating PD-L1 and TGF-β expression, it was predicted that TAM may possess the capacity to inhibit PD-L1 and TGF-β protein expression in tumors[48–50]. To prove this, Western blot assay was first used to evaluate whether this prediction was right in 4T1 breast cancer cells. As results showed, a high dosage of TAM effectively activated the AMPK pathway and depressed PD-L1 and TGF-β protein expression (Supporting Information Fig. S2). All in all, TAM could inhibit PD-L1 and TGF-β protein expression at a high dosage.

As previously reported, conjugating TAM with mitochondria-targeting agents may also decrease the dosage of TAM needed to induce mitochondria dysfunction[30]. Moreover, cationic TPP possessed ideal tumor mitochondria targeting capacity[39,51]. Thus, we believed that conjugating TAM with TPP may be more effective than TAM in downregulating PD-L1 and TGF-β protein expression (Fig. 1A). According to this speculation, TPP-TAM was prepared and its correct synthesis was confirmed by ^{1}H NMR and HR-MS (Supporting Information Figs. S3–S5). Following this, the capacity of TPP-TAM in inhibiting mitochondrial complex I was evaluated, showing that TPP-TAM more effectively inhibited the activity of mitochondrial complex I with a decreased half inhibition dosage of about 14.3% of TAM *in vitro* (Fig. 1B). Besides, the mitochondrial membrane potential of 4T1 cells was also decreased by 2 μmol/L TPP-TAM, which was as effective as 20 μmol/L TAM (Fig. 1C). Due to the proved effects of TPP-TAM on mitochondrial complex I, TPP-TAM time-dependently raised the ADP/ATP ratio, which then effectively induced the amplified AMPK phosphorylation at a relatively low concentration of about 1 μmol/L (Fig. 1D–F). Then, TPP-TAM efficiently downregulated PD-L1 and TGF-β protein expression in 4T1 cells *in vitro*, which was only about 5% of the concentration of TAM needed (TAM 20 μmol/L *vs* TPP-TAM 1 μmol/L) (Fig. 1G–I, Fig. S2). All in all, TPP-TAM rather than TAM may work as a more potent PD-L1 and TGF-β dual-inhibitor.

3.2. Preparation and characterization of TPP-TAM@Alb nanoparticles

To better deliver the hydrophobic drug TPP-TAM *in vivo*, TPP-TAM@Alb nanoparticles were prepared by using Alb to encapsulate TPP-TAM *via* a one-step hydrophobic and hydrophilic

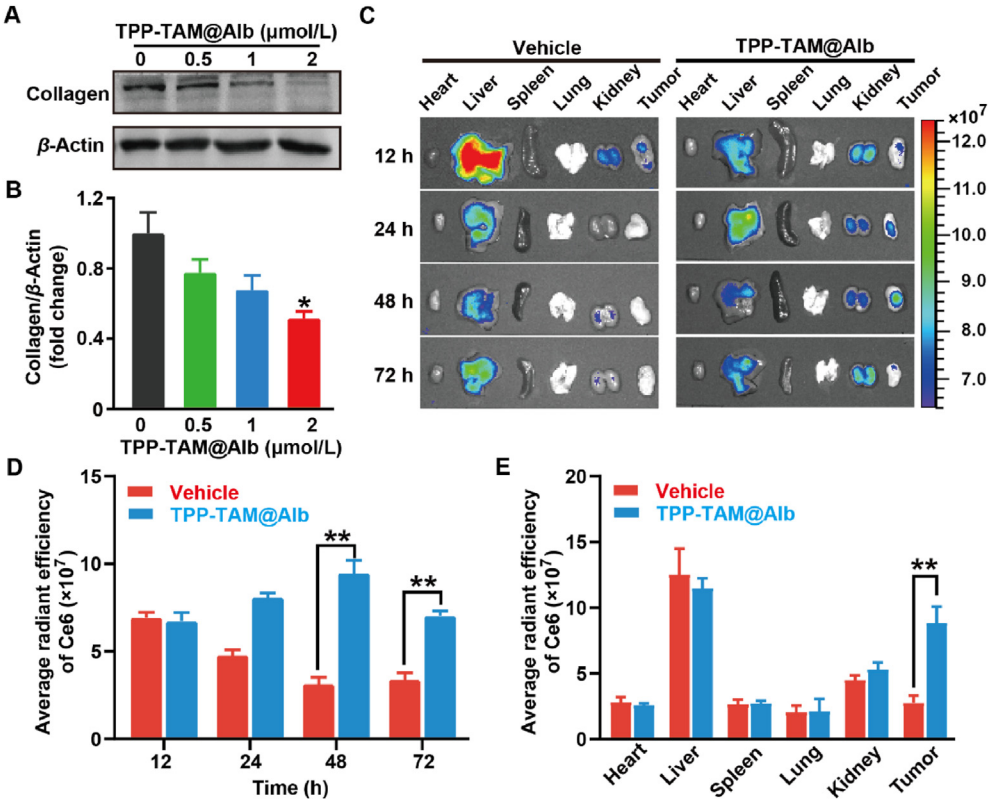

Figure 4 Effects of TPP-TAM@Alb on the accumulation of Ce6 co-loaded PTX@Alb in 4T1 tumors. (A) The typical image of collagen I detected by Western blot assay after different treatments. (B) Quantification of the expression levels of collagen I after various treatments ($n = 3$). (C) Near-infrared fluorescence images of 4T1 tumor-bearing mice at 12, 24, 48, and 72 h after the intravenous injection of Ce6 co-loaded PTX@Alb (Ce6 concentration: 0.6 mg/kg, PTX concentration: 5 mg/kg), which was pre-treated with Vehicle or TPP-TAM@Alb 24 h before (TPP-TAM concentration: 5 mg/kg). (D, E) Corresponding quantification of the fluorescence signal of Ce6 co-loaded PTX@Alb from organs and tumors ($n = 3$). All data are presented as mean ± SD. $^{**}P < 0.01$.

self-assembly strategy as previously reported (Fig. 2A)[35,41,45]. TEM image showed that the morphology of TPP-TAM@Alb was nearly spherical shape (Fig. 2B). The particle size of TPP-TAM@Alb was 202.2 ± 15.3 nm (Fig. 2B). As examined by the UV−Vis absorbance spectra of TPP-TAM, the drug loading capacity of TPP-TAM in TPP-TAM@Alb nanoparticles was 1.56 ± 0.35%. Besides, it was also revealed that TPP-TAM showed relatively desirable stability by detecting the hydrodynamic size and polydispersity index of TPP-TAM using PBS or FBS at pH 7.4 (Fig. 2C and D). Moreover, as time went on, most TPP-TAM was released from TPP-TAM@Alb nanoparticles at 48 h (Fig. 2E). To sum up, TPP-TAM@Alb nanoparticles possessed favorable particle size distribution and relatively ideal particle stability.

3.3. The ability of TPP-TAM@Alb in promoting the tumor-killing capacity of PTX@Alb in vitro

Subsequently, the combination effects of TPP-TAM@Alb and PTX@Alb on regulating tumor cell proliferation and apoptosis were assessed by flow cytometry (Fig. 2F). As results indicated, amounts of reactive oxygen species (ROS) were generated when 4T1 cells were co-treated with PTX@Alb and TPP-TAM@Alb, while PTX@Alb or TPP-TAM@Alb alone could only generated less ROS (Supporting Information Fig. S6). Besides, TPP-TAM@Alb and PTX@Alb co-treatment rather than TPP-TAM@Alb or PTX@Alb treatment alone more effectively induced tumor cell apoptosis, which then was further confirmed by the CCK-8-based cell viability assay and Western blot assay of Bcl-2 (Fig. 2F and G, Supporting Information Figs. S7−S9). Then, the effects of TPP-TAM@Alb or PTX@Alb on tumor cell growth and proliferation were also evaluated (Fig. 2H and I). As results indicated, TPP-TAM@Alb or PTX@Alb treatment alone both could slightly decrease the formation of 4T1 cell clones, while TPP-TAM@Alb and PTX@Alb combination therapy almost totally inhibited the formation of 4T1 cell clones (Fig. 2H and I). To evaluate whether the high expression of estrogen receptors in breast cancer cells would affect the capacity of TPP-TAM@Alb in sensitizing PTX@Alb-mediated chemotherapy, MCF-7 breast cancer cells were used (Supporting Information Fig. S10). Similar to the results indicated in 4T1 cells, TPP-TAM@Alb also obviously increased the tumor cell killing capacity of PTX@Alb in MCF-7 cells (Fig. S10). In a word, TPP-TAM@Alb promoted the tumor-

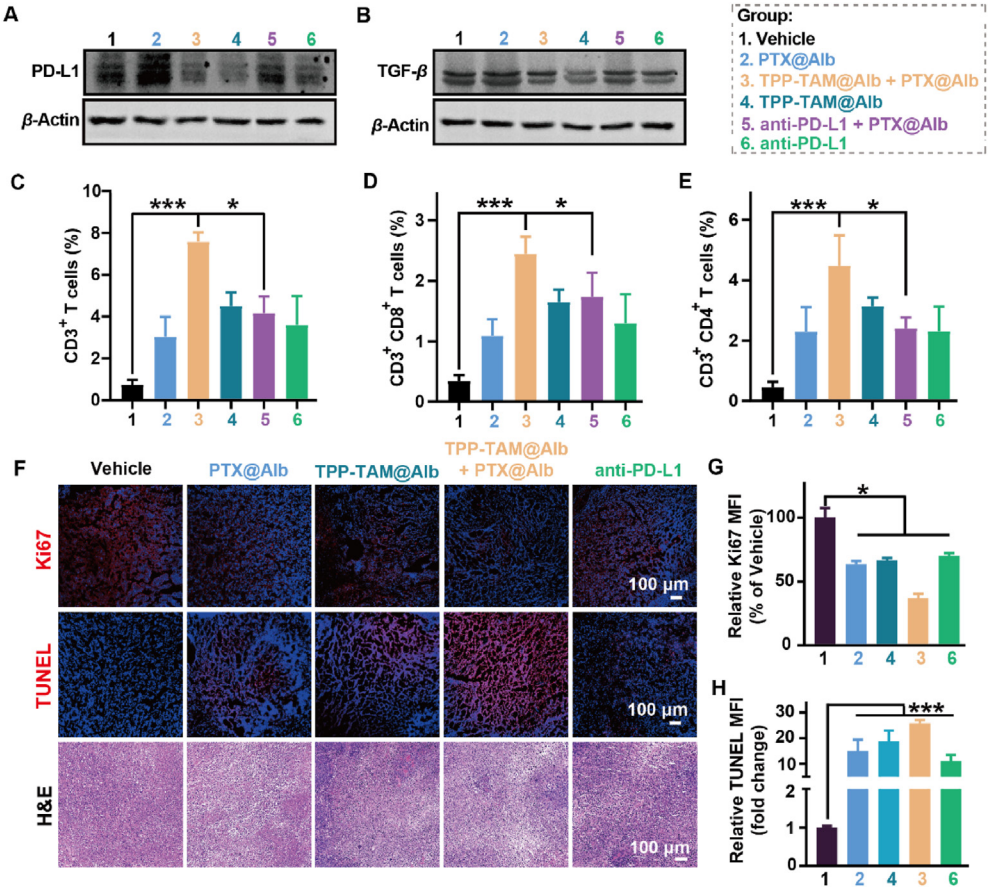

Figure 5 TPP-TAM@Alb nanoparticles reduced the expression of PD-L1 and TGF-β protein to amplify T cell infiltration in 4T1 subcutaneous tumors for enhancing the tumor cell killing activity of PTX@Alb. (A, B) The typical image of the PD-L1 and TGF-β proteins in 4T1 tumors detected by Western blot assay after different treatments. (C−E) Quantification of the amounts of $CD3^+$, $CD8^+$, and $CD4^+$ T cells in 4T1 tumors by the flow cytometry measurements after receiving various treatments ($n = 5$). (F) The representative immunofluorescence images of Ki67 protein, TUNEL, and H&E staining after PTX@Alb, TPP-TAM@Alb, anti-PD-L1 antibody, or PTX@Alb and TPP-TAM@Alb combination therapy, scale bar = 100 μm. (G, H) Quantification of the relative Ki67 and TUNEL mean fluorescence intensity (MFI) after different treatments ($n = 3$). All data are presented as mean ± SD. *$P < 0.05$ and ***$P < 0.001$.

killing capacity of PTX@Alb *in vitro* in an estrogen receptor-independent behavior.

3.4. TPP-TAM@Alb inhibited PD-L1 and TGF-β expression and induced ICD

Currently, PTX@Alb is used as a typical FDA-approved nano-system for treating breast cancer in clinical[43]. Although it could induce ICD to enhance the tumor immune activity, the defects of PTX@Alb in inhibiting TGF-β expression, as well as its weak capacity in upregulating PD-L1, still could lead to immune tolerance[5,37,52]. As we just proved above, TPP-TAM could effectively depress PD-L1 and TGF-β expression simultaneously (Fig. 1). Thus, we suspected that TPP-TAM@Alb may make up the defects of PTX@Alb in regulating PD-L1 and TGF-β expression. As results indicated, PTX@Alb could not decrease or even slightly increase the expression of PD-L1 and TGF-β expression in 4T1 and MCF-7 cells *in vitro*, while the combination therapy of PTX@Alb and TPP-TAM@Alb depressed the expression of these two proteins (Fig. 3A−D, Supporting Information Fig. S11). Following this, to confirm whether TPP-TAM@Alb inhibited PD-L1 and TGF-β expression by the same mechanism as TAM, Com C was used to depress the AMPK pathway (Fig. 3E−G). Similarly, after Com C treatment, the capacity of TPP-TAM@Alb in depressing PD-L1 and TGF-β expression was reversed, meaning that TPP-TAM@Alb regulated PD-L1 and TGF-β expression at least partly by affecting the AMPK pathway (Fig. 3E−G, Supporting Information Fig. S12). Then, we evaluated the effects of TPP-TAM@Alb on inducing ICD, showing that TPP-TAM@Alb could also enhance the surface location of CRT and induce the secretion of HMGB1 (Fig. 3H). In a word, TPP-TAM@Alb effectively inhibited PD-L1 and TGF-β expression and induced ICD, which may further sensitize PTX@Alb-based chemo-immunotherapy *in vivo*.

3.5. TPP-TAM@Alb decreased collagen distribution in 4T1 tumors to enhance the accumulation of PTX@Alb

In solid tumors, due to the enhanced TGF-β expression and secretion, amounts of collagen were generated by tumor cells or fibroblasts[24,53−55]. As we proved above, TPP-TAM@Alb decreased TGF-β *in vitro* (Fig. 3). Thus, the expression levels of collagen in 4T1 cells may also be depressed by TPP-TAM@Alb. To prove this, Western blot assay was used, showing that TPP-TAM@Alb dose-dependently inhibited collagen expression in 4T1 cells *in vitro* (Fig. 4A and B). Then, the effects of TPP-TAM@Alb on the accumulation of PTX@Alb in 4T1 tumors were also evaluated by using Ce6 co-loaded PTX@Alb (Ce6 used as a drug indicator) (Fig. 4). Generally, the accumulation of Ce6 co-loaded PTX@Alb in tumors pre-treated with TPP-TAM@Alb

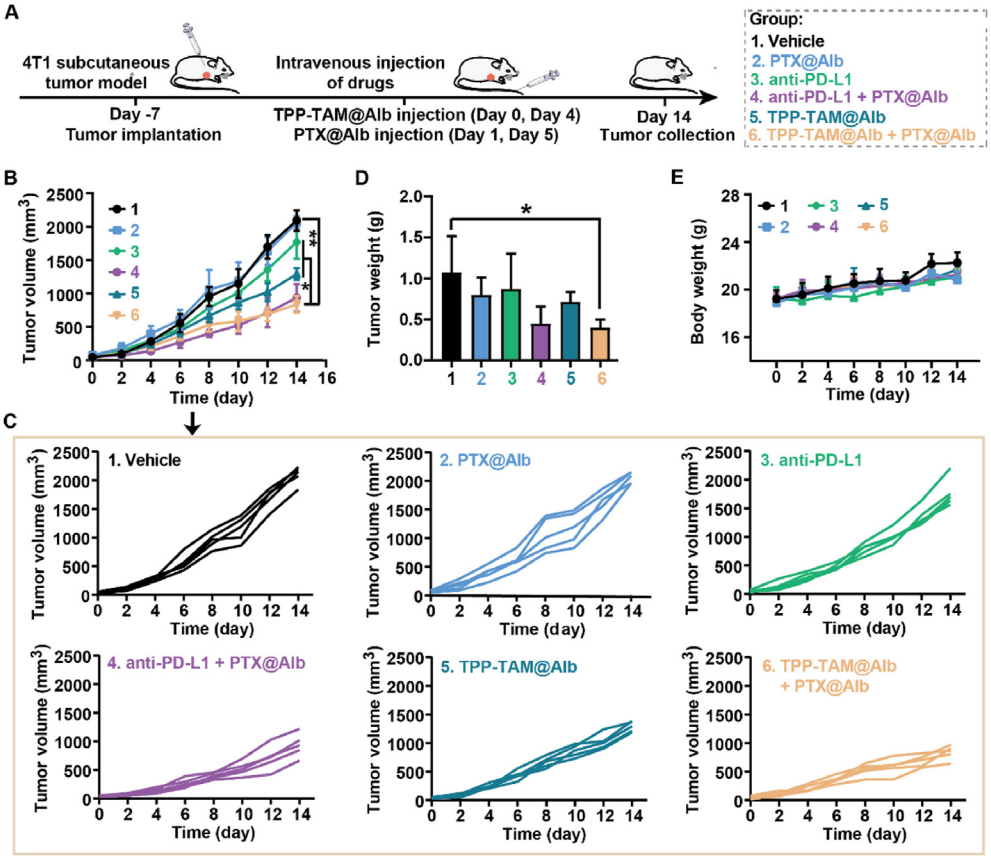

Figure 6 Evaluation of the combination anti-tumor efficacy of PTX@Alb and TPP-TAM@Alb in subcutaneously transplanted 4T1 tumor-bearing mice. (A) Schematic diagram of the combination treatment process of PTX@Alb and TPP-TAM@Alb in 4T1 tumor-bearing mice. (B, C) The growth curve of 4T1 tumors after receiving various treatments ($n = 5$). (D) The weight of 4T1 tumor collected on Day 14 after various treatments ($n = 5$). (E) Changes in the body weight of 4T1 tumor-bearing mice after receiving various treatments ($n = 5$). All data are presented as mean ± SD. $^*P < 0.05$ and $^{**}P < 0.01$.

was about 2 fold that of TPP-TAM@Alb un-treated group, which was similar to the results of the PTX concentrations detected in 4T1 tumors by HPLC (Fig. 4C−E, Supporting Information Fig. S13). Most important of all, the accumulation behavior of Ce6 co-loaded PTX@Alb in the normal tissues like the heart, lung, kidney, spleen, and liver was almost not affected when pre-treated by TPP-TAM@Alb (Fig. 4C−E). All in all, TPP-TAM@Alb selectively and effectively enhanced the accumulation of PTX@Alb in 4T1 tumors.

3.6. TPP-TAM@Alb and PTX@Alb co-treatment enhanced the infiltration of T cells in tumors and induced obvious cell apoptosis

Like the evaluation of PD-L1 and TGF-β protein expression *in vitro*, the capacity of TPP-TAM@Alb in affecting PD-L1 and TGF-β protein expression *in vivo* was also detected by the Western blot assay (Fig. 5A and B). As results indicated, the expression levels of PD-L1 and TGF-β protein *in vivo* after TPP-TAM@Alb treatment or TPP-TAM@Alb and PTX@Alb co-treatment was also similarly depressed, while PTX@Alb possessed no such capacity (Fig. 5A and B, Supporting Information Fig. S14). Considering the role of PD-L1 and TGF-β protein in inducing immune tolerance, we evaluated the effects of TPP-TAM@Alb in reversing immune resistance by using flow cytometry (Fig. 5C−E). Generally, after PTX@Alb or TPP-TAM@Alb treatment, the infiltration of $CD3^+$, $CD4^+$, and $CD8^+$ T cells was slightly increased (Fig. 5C−E). When treating PTX@Alb together with TPP-TAM@Alb rather than anti-PD-L1 antibody alone, the most obvious enhanced infiltration of T cells in 4T1 tumors was realized, meaning that TPP-TAM@Alb may best enhance chemo-immunotherapy mediated by PTX@Alb (Fig. 5C−E). Then, TUNEL staining, H&E staining, and Ki67 staining of tumor tissue

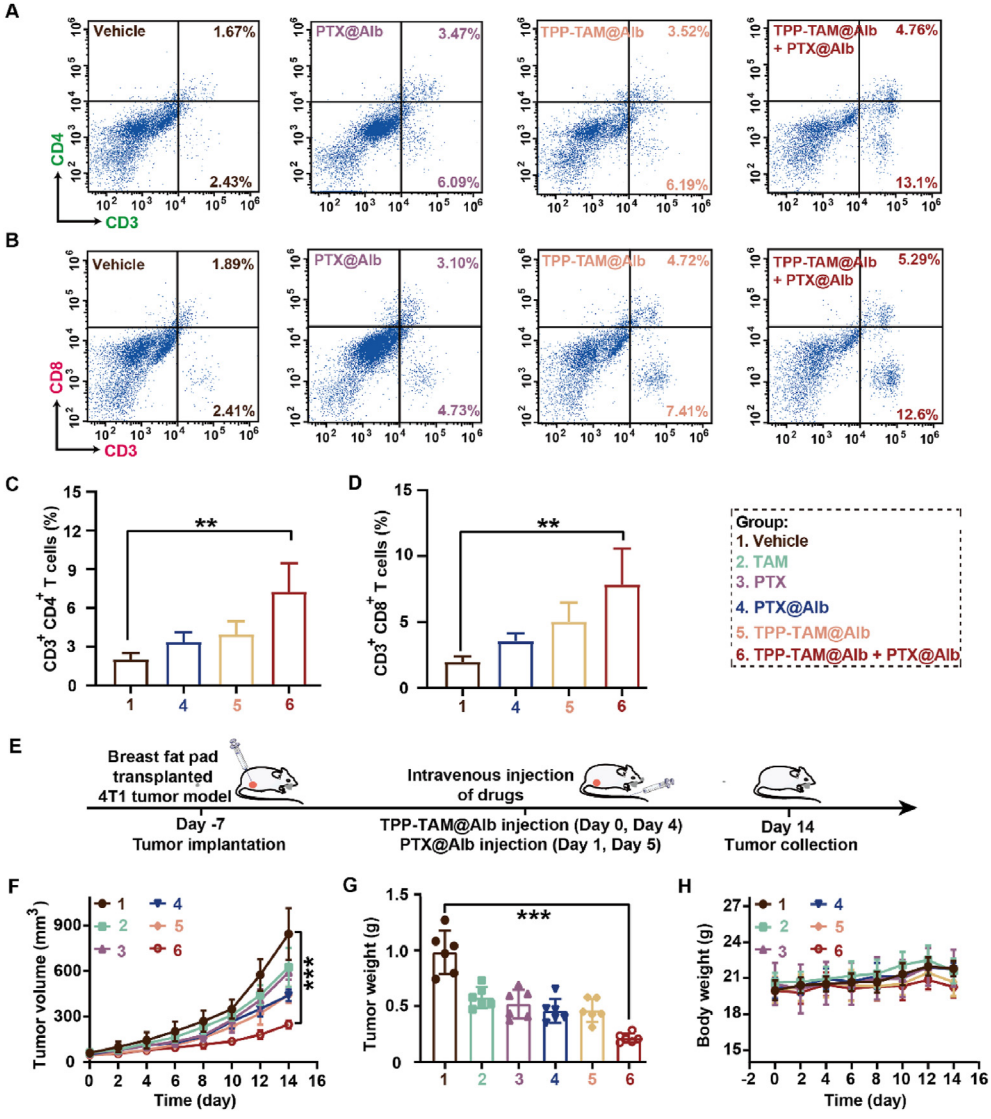

Figure 7 Evaluation of the combination anti-tumor efficacy of PTX@Alb and TPP-TAM@Alb in breast fat pad transplanted 4T1 tumors-bearing mice. (A−D) Quantification of the amounts of $CD3^+$, $CD8^+$, and $CD4^+$ T cells in 4T1 tumors by the flow cytometry measurements after receiving various treatments ($n = 5$). (E) Schematic diagram of the combination treatment process of PTX@Alb and TPP-TAM@Alb in breast fat pad transplanted 4T1 tumors-bearing mice. (F) The growth curve of 4T1 tumors after receiving various treatments ($n = 6$). (G) The weight of 4T1 tumor collected on Day 14 after various treatments ($n = 6$). (H) Changes in the body weight of 4T1 tumor-bearing mice after receiving various treatments ($n = 6$). All data are presented as mean ± SD. $^{**}P < 0.01$ and $^{***}P < 0.001$.

sections were also performed to evaluate the tumor cell proliferation and apoptosis after various treatments (Fig. 5F−H). As illustrated in Fig. 5F−H, the combination therapy of TPP-TAM@Alb and PTX@Alb lead to the most obvious cell apoptosis, followed by TPP-TAM@Alb or PTX@Alb treatment. To sum up, TPP-TAM@Alb could better reverse the immune tolerance induced by PTX@Alb to enhance the immune-killing effect of T cells and induce the most obvious tumor cell apoptosis.

3.7. TPP-TAM@Alb and PTX@Alb co-treatment inhibited 4T1 tumor growth

Considering the proven fact that TPP-TAM@Alb could enhance the accumulation of PTX@Alb in tumors and reverse the possible immune tolerance induced by PTX@Alb-mediated chemo-immunotherapy, we further evaluated the combination anti-tumor efficacy of TPP-TAM@Alb and PTX@Alb in subcutaneously implanted 4T1 tumors (Fig. 6A). As shown in Fig. 6B and C, the volume of 4T1 tumors in the vehicle group continued to grow as time goes on. After the treatment of PTX@Alb or TPP-TAM@Alb, the tumor growth rate was only slightly decreased (Fig. 6B and C). When co-treating 4T1 tumor-bearing mice together with TPP-TAM@Alb and PTX@Alb, the growth of 4T1 tumors was slowed down with a tumor growth inhibition rate of about 65% (Fig. 6B and C). Besides, the tumor weight of TPP-TAM@Alb-treated 4T1 tumors decreased from 1.08 ± 0.49 g to 0.72 ± 0.14 g, while it was 0.41 ± 0.10 g for TPP-TAM@Alb and PTX@Alb co-treatment group, meaning that TPP-TAM@Alb and PTX@Alb co-treatment most obviously inhibited 4T1 tumor growth (Fig. 6D, Supporting Information Fig. S15). Meanwhile, it was also revealed that TPP-TAM@Alb or TPP-TAM@Alb and PTX@Alb co-therapy effectively inhibited the formation of 4T1 tumor lung metastasis foci, while PTX@Alb possessed no such capacity (Supporting Information Fig. S16). Moreover, the body weight of Balb/C mice after TPP-TAM@Alb treatment didn't show any obvious changes, suggesting that TPP-TAM@Alb possessed ideal biosafety (Fig. 6E). To sum up, TPP-TAM@Alb nanoparticles could better enhance the anti-tumor efficacy of PTX@Alb-mediated chemo-immunotherapy.

To further evaluate the combination anti-tumor efficacy of TPP-TAM@Alb and PTX@Alb in local solid tumors, the breast fat pad implanted local 4T1 tumors were also used (Fig. 7). As shown in Fig. 7A−D, after PTX@Alb or TPP-TAM@Alb treatment, the infiltration of $CD3^+$, $CD4^+$, and $CD8^+$ T cells in 4T1 tumors was slightly increased, which then was most effectively enhanced when co-treated PTX@Alb with TPP-TAM@Alb. Following this, the growth of breast fat pad implanted local 4T1 tumors was investigated (Fig. 7E). As indicated, PTX@Alb or TPP-TAM@Alb only slightly inhibited the growth of 4T1 tumors, which was a little better than free PTX or TAM-treated mice (Fig. 7F). When co-treating 4T1 tumor-bearing mice together with TPP-TAM@Alb and PTX@Alb, the growth of 4T1 tumors was slowed down with a tumor growth inhibition rate of about 71% (Fig. 7F, Supporting Information Fig. S17). Besides, the tumor weight of TPP-TAM@Alb and PTX@Alb co-treatment group decreased from 0.98 ± 0.19 g to 0.21 ± 0.04 g, indicating that TPP-TAM@Alb and PTX@Alb co-treatment could more obviously inhibit the growth of breast fat pad implanted 4T1 tumor (Fig. 7G and H, Supporting Information Fig. S18). To sum up, TPP-TAM@Alb nanoparticles could better enhance the anti-tumor efficacy of PTX@Alb-mediated chemo-immunotherapy.

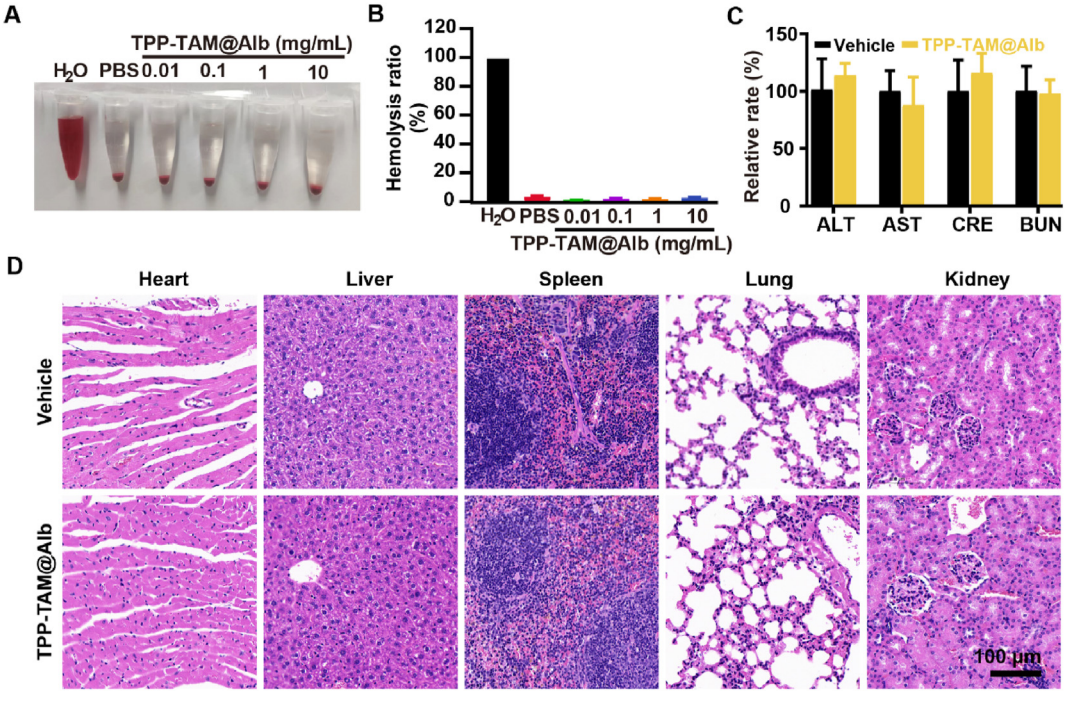

Figure 8 Evaluation of the biosafety of TPP-TAM@Alb. (A) The typical photo of the hemolytic test treated by various concentrations of TPP-TAM@Alb. (B) Quantification of the hemolysis ratio of RBCs treated by various concentrations of TPP-TAM@Alb ($n = 3$). (C) Detection of the changes of ALT, CRE, AST, and BUN in the serum collected from BALB/c mice receiving TPP-TAM@Alb (TPP-TAM concentration, 5 mg/kg) for 24 h to predict the influence of TPP-TAM@Alb on the liver and spleen function ($n = 3$). (D) Representative H&E images of the heart, lung, liver, spleen, and kidney collected from the healthy mice treated by Vehicle (0.9% saline) or TPP-TAM@Alb (TPP-TAM concentration, 5 mg/kg) for 14 days (twice a week), scale bar = 100 μm. All data are presented as mean ± SD.

3.8. *Biosafety evaluation of TPP-TAM@Alb nanoparticles*

At last, the biosafety of TPP-TAM@Alb nanoparticles was evaluated (Fig. 8). As results of the hemolysis assay showed, TPP-TAM@Alb possessed ideal hemocompatibility since TPP-TAM@Alb did not induce obvious hemolysis of red blood cells (Fig. 8A and B). Then, it was revealed that TPP-TAM@Alb did not affect the function of liver and spleen by evaluating the influence of TPP-TAM@Alb on ALT, BUN, CRE, and AST (Fig. 8C). Moreover, the results of H&E staining also indicated that no significant pathological changes of liver, lung, spleen, kidney, and heart were caused by TPP-TAM@Alb (Fig. 8D, Supporting Information Fig. S19). Thus, TPP-TAM@Alb nanoparticles possessed the desired biosecurity.

4. Conclusions

In this study, it was newly revealed that TAM, a typical adjuvant chemotherapy drug used for the endocrine treatment of a variety of ER-positive breast cancers, could also be used as a TGF-β and PD-L1 dual-inhibitor. Following this, TPP-TAM was chemically prepared by conjugating TAM with TPP, which was more effective than TAM in inhibiting TGF-β and PD-L1 expression (TAM 20 μmol/L *vs.* TPP-TAM 1 μmol/L). Then, to better deliver TPP-TAM to 4T1 tumors, TPP-TAM@Alb was prepared by self-assembling Alb with TPP-TAM. By doing this, TPP-TAM@Alb effectively decreased TGF-β and collagen expression *in vivo* to enhance the accumulation of Ce6 co-loaded PTX@Alb in 4T1 tumors. Apart from this, the T cell infiltration in 4T1 tumors was most obviously enhanced after the combination treatment of PTX@Alb and TPP-TAM@Alb rather than PTX@Alb itself, which was at least partly induced by the TPP-TAM@Alb down-regulated TGF-β and PD-L1 expression. At last, the most ideal anti-tumor efficacy was obtained when treated by PTX@Alb and TPP-TAM@Alb together. Thus, in this research, we newly proposed the potential of using TAM and its derivants as substitutes for the clinically used PD-L1 or TGF-β antibody, which may expand the future clinical application of TAM in tumor therapy.

Acknowledgments

This study was supported by the National Natural Science Foundation of China (22377093), the Zhejiang Provincial Natural Science Foundation for Distinguished Young Scholar (LR23C100001, China), and the Zhejiang Qianjiang Talent Plan (QJD20020224, China).

Author contributions

Zaigang Zhou: Conceptualization, Data curation, Writing − original draft, Writing − review & editing, Investigation. Wenjuan Luo: Data curation, Investigation. Chunjuan Zheng: Data curation, Investigation. Haoxiang Wang: Data curation, Formal analysis, Investigation. Rui Hu: Investigation, Methodology. Hui Deng: Funding acquisition, Supervision. Jianliang Shen: Funding acquisition, Project administration, Supervision, Writing − review & editing.

Conflicts of interest

The authors have no conflicts of interest to declare.

Appendix A. Supporting information

Supporting information to this article can be found online at https://doi.org/10.1016/j.apsb.2024.05.028.

References

1. Sung H, Ferlay J, Siegel RL, Laversanne M, Soerjomataram I, Jemal A, et al. Global cancer statistics 2020: globocan estimates of incidence and mortality worldwide for 36 cancers in 185 countries. *CA Cancer J Clin* 2021;**71**:209−49.
2. Gou SQ, Chen NX, Wu XA, Zu MH, Yi SX, Ying BW, et al. Multi-responsive nanotheranostics with enhanced tumor penetration and oxygen self-producing capacities for multimodal synergistic cancer therapy. *Acta Pharm Sin B* 2022;**12**:406−23.
3. Drusbosky L, Nangia C, Nguyen A, Szeto C, Newton Y, Spilman P, et al. Complete response to avelumab and IL-15 superagonist N-803 with Abraxane in merkel cell carcinoma: a case study. *J Immunother Cancer* 2020;**8**:e001098.
4. Gianni L, Mansutti M, Anton A, Calvo L, Bisagni G, Bermejo B, et al. Comparing neoadjuvant Nab-paclitaxel *vs* paclitaxel both followed by anthracycline regimens in women with ERBB2/HER2-negative breast cancer-the evaluating treatment with neoadjuvant Abraxane (ETNA) trial: a randomized phase 3 clinical trial. *JAMA Oncol* 2018;**4**:302−8.
5. Vennin C, Cattaneo CM, Bosch L, Vegna S, Ma XH, Damstra HGJ, et al. Taxanes trigger cancer cell killing *in vivo* by inducing non-canonical T cell cytotoxicity. *Cancer Cell* 2023;**41**:1170−85.
6. Zhan MS, Qiu JR, Fan Y, Chen L, Guo YQ, Wang ZQ, et al. Phosphorous dendron micelles as a nanomedicine platform for cooperative tumor chemoimmunotherapy *via* synergistic modulation of immune cells. *Adv Mater* 2023;**35**:e2208277.
7. Zhou ZG, Zhang BL, Wang SS, Zai WJ, Yuan AH, Hu YQ, et al. Perfluorocarbon nanoparticles mediated platelet blocking disrupt vascular barriers to improve the efficacy of oxygen-sensitive antitumor drugs. *Small* 2018;**14**:e1801694.
8. Zi YX, Yang KY, He JH, Wu ZM, Liu JP, Zhang WL. Strategies to enhance drug delivery to solid tumors by harnessing the EPR effects and alternative targeting mechanisms. *Adv Drug Deliv Rev* 2022;**188**:114449.
9. Mi Z, Yao Q, Qi Y, Zheng JH, Liu JH, Liu ZG, et al. Salmonella-mediated blood−brain barrier penetration, tumor homing and tumor microenvironment regulation for enhanced chemo/bacterial glioma therapy. *Acta Pharm Sin B* 2023;**13**:819−33.
10. Luo M, Wang F, Zhang H, To KKW, Wu SC, Chen Z, et al. Mitomycin C enhanced the efficacy of PD-L1 blockade in non-small cell lung cancer. *Signal Transduct Target Ther* 2020;**5**:141.
11. Nagaraju GP, Malla RR, Basha R, Motofei IG. Contemporary clinical trials in pancreatic cancer immunotherapy targeting PD-1 and PD-L1. *Semin Cancer Biol* 2022;**86**:616−21.
12. Chen Q, Xia R, Zheng WW, Zhang LY, Li P, Sun XW, et al. Metronomic paclitaxel improves the efficacy of PD-1 monoclonal antibodies in breast cancer by transforming the tumor immune microenvironment. *Am J Transl Res* 2020;**12**:519−30.
13. Hu C, Song YJ, Zhang YW, He SQ, Liu XY, Yang XT, et al. Sequential delivery of PD-1/PD-L1 blockade peptide and IDO inhibitor for immunosuppressive microenvironment remodeling *via* an MMP-2 responsive dual-targeting liposome. *Acta Pharm Sin B* 2023;**13**:2176−87.
14. Cha JH, Yang WH, Xia WY, Wei YK, Chan LC, Lim SO, et al. Metformin promotes antitumor immunity *via* endoplasmic-reticulum-associated degradation of PD-L1. *Mol Cel* 2018;**71**:606−20.
15. Shi YF, Lim SK, Liang QR, Iyer SV, Wang HY, Wang ZL, et al. Gboxin is an oxidative phosphorylation inhibitor that targets glioblastoma. *Nature* 2019;**567**:341−6.
16. Mills EL, Kelly B, O'Neill LAJ. Mitochondria are the powerhouses of immunity. *Nat Immunol* 2017;**18**:488−98.
17. Zhang JN, Zhang Z, Huang ZL, Li ML, Yang F, Wu ZQ, et al. Isotoosendanin exerts inhibition on triple-negative breast cancer through

abrogating TGF-β-induced epithelial-mesenchymal transition *via* directly targeting TGFβR1. *Acta Pharm Sin B* 2023;**13**:2990−3007.
18. Zhou ZG, Liu Y, Jiang X, Zheng CJ, Luo WJ, Xiang XL, et al. Metformin modified chitosan as a multi-functional adjuvant to enhance cisplatin-based tumor chemotherapy efficacy. *Int J Biol Macromol* 2023;**224**:797−809.
19. Zhou ZG, Zheng CJ, Liu Y, Luo WJ, Deng H, Shen JL. Chitosan biguanide induced mitochondrial inhibition to amplify the efficacy of oxygen-sensitive tumor therapies. *Carbohydr Polym* 2022;**295**:119878.
20. Bonekamp NA, Peter B, Hillen HS, Felser A, Bergbrede T, Choidas A, et al. Small-molecule inhibitors of human mitochondrial DNA transcription. *Nature* 2020;**588**:712−6.
21. Zhou ZG, Chen JS, Liu Y, Zheng CJ, Luo WJ, Chen LL, et al. Cascade two-stage tumor re-oxygenation and immune re-sensitization mediated by self-assembled albumin-sorafenib nanoparticles for enhanced photodynamic immunotherapy. *Acta Pharm Sin B* 2022;**12**:4204−23.
22. Li JH, Huang LJ, Zhou HL, Shan YM, Chen FM, Lehto VP, et al. Engineered nanomedicines block the PD-1/PD-L1 axis for potentiated cancer immunotherapy. *Acta Pharmacol Sin* 2022;**43**:2749−58.
23. Han HJ, Hou Y, Chen XH, Zhang PS, Kang M, Jin Q, et al. Metformin-induced stromal depletion to enhance the penetration of Gemcitabine-loaded magnetic nanoparticles for pancreatic cancer targeted therapy. *J Am Chem Soc* 2020;**142**:4944−54.
24. Lan Y, Moustafa M, Knoll M, Xu CX, Furkel J, Lazorchak A, et al. Simultaneous targeting of TGF-β/PD-L1 synergizes with radiotherapy by reprogramming the tumor microenvironment to overcome immune evasion. *Cancer Cell* 2021;**39**:1388−403.
25. Meng XM, Nikolic-Paterson DJ, Lan HY. TGF-β: the master regulator of fibrosis. *Nat Rev Nephrol* 2016;**12**:325−38.
26. Qi GH, Zhou Y, Zhang XP, Yu JQ, Li X, Cao XX, et al. Cordycepin promotes browning of white adipose tissue through an AMP-activated protein kinase (AMPK)-dependent pathway. *Acta Pharm Sin B* 2019;**9**:135−43.
27. Costa A, Kieffer Y, Scholer-Dahirel A, Pelon F, Bourachot B, Cardon M, et al. Fibroblast heterogeneity and immunosuppressive environment in human breast cancer. *Cancer Cell* 2018;**33**:463−79.
28. Valkenburg KC, de Groot AE, Pienta KJ. Targeting the tumour stroma to improve cancer therapy. *Nat Rev Clin Oncol* 2018;**15**:366−81.
29. Zhou ZG, Zhang BL, Zai WJ, Kang L, Yuan AH, Hu YQ, et al. Perfluorocarbon nanoparticle-mediated platelet inhibition promotes intratumoral infiltration of T cells and boosts immunotherapy. *Proc Natl Acad Sci U S A* 2019;**116**:11972−7.
30. Daurio NA, Tuttle SW, Worth AJ, Song EY, Davis JM, Snyder NW, et al. AMPK activation and metabolic reprogramming by Tamoxifen through estrogen receptor-independent mechanisms suggests new uses for this therapeutic modality in cancer treatment. *Cancer Res* 2016;**76**:3295−306.
31. Li ML, Shao YJ, Kim JH, Pu ZJ, Zhao XZ, Huang HQ, et al. Unimolecular photodynamic O_2-economizer to overcome hypoxia resistance in phototherapeutics. *J Am Chem Soc* 2020;**142**:5380−8.
32. Yan Y, Du CC, Duan XX, Yao XH, Wan JJ, Jiang ZM, et al. Inhibiting collagen I production and tumor cell colonization in the lung *via* miR-29a-3p loading of exosome-/liposome-based nanovesicles. *Acta Pharm Sin B* 2022;**12**:939−51.
33. Early Breast Cancer Trialists' Collaborative G. Aromatase inhibitors versus tamoxifen in premenopausal women with oestrogen receptor-positive early-stage breast cancer treated with ovarian suppression: a patient-level meta-analysis of 7030 women from four randomised trials. *Lancet Oncol* 2022;**23**:382−92.
34. Yi L, Jiang X, Zhou ZG, Xiong W, Xue F, Liu Y, et al. A hybrid nanoadjuvant simultaneously depresses PD-L1/TGF-β1 and activates cGAS−STING pathway to overcome radio-immunotherapy resistance. *Adv Mater* 2024;**36**:e2304328.
35. Jiang X, Yi L, Li C, Wang HX, Xiong W, Li Y, et al. Mitochondrial disruption nanosystem simultaneously depressed programmed death ligand-1 and transforming growth factor-β to overcome photodynamic immunotherapy resistance. *ACS Nano* 2024;**18**:3331−48.
36. Zhou ZG, Jiang X, Yi L, Li C, Wang HX, Xiong W, et al. Mitochondria energy metabolism depression as novel adjuvant to sensitize radiotherapy and inhibit radiation induced-pulmonary fibrosis. *Adv Sci* 2024;**11**:e2401394.
37. Zhou ZG, Wang HX, Li J, Jiang X, Li ZP, Shen JL. Recent progress, perspectives, and issues of engineered PD-L1 regulation nano-system to better cure tumor: a review. *Int J Biol Macromol* 2023;**254**:127911.
38. Petri BJ, Piell KM, South Whitt GC, Wilt AE, Poulton CC, Lehman NL, et al. HNRNPA2B1 regulates tamoxifen- and fulvestrant-sensitivity and hallmarks of endocrine resistance in breast cancer cells. *Cancer Lett* 2021;**518**:152−68.
39. Wang SJ, Zhou ZG, Hu R, Dong MY, Zhou XB, Ren SY, et al. Metabolic intervention liposome boosted lung cancer radio-immunotherapy *via* hypoxia amelioration and PD-L1 restraint. *Adv Sci* 2023:e2207608.
40. Lin X, Li L, Li SJ, Li QY, Xie DD, Zhou ML, et al. Targeting the opening of mitochondrial permeability transition pores potentiates nanoparticle drug delivery and mitigates cancer metastasis. *Adv Sci* 2021;**8**:2002834.
41. Jiang CX, Cheng H, Yuan AH, Tang XL, Wu JH, Hu YQ. Hydrophobic IR780 encapsulated in biodegradable human serum albumin nanoparticles for photothermal and photodynamic therapy. *Acta Biomater* 2015;**14**:61−9.
42. Sreekanth V, Bansal S, Motiani RK, Kundu S, Muppu SK, Majumdar TD, et al. Design, synthesis, and mechanistic investigations of bile acid−tamoxifen conjugates for breast cancer therapy. *Bioconjug Chem* 2013;**24**:1468−84.
43. Meng LT, Gan SJ, Zhou Y, Cheng YL, Ding YW, Tong XQ, et al. Oxygen-rich chemotherapy *via* modified Abraxane to inhibit the growth and metastasis of triple-negative breast cancer. *Biomater Sci* 2018;**7**:168−77.
44. Tang XL, Wang GJ, Shi RS, Jiang K, Meng LT, Ren H, et al. Enhanced tolerance and antitumor efficacy by docetaxel-loaded albumin nanoparticles. *Drug Deliv* 2015;**23**:2686−96.
45. Liu Y, Zhou ZG, Hou JT, Xiong W, Kim H, Chen JS, et al. Tumor selective metabolic reprogramming as a prospective PD-L1 depression strategy to reactivate immunotherapy. *Adv Mater* 2022;**34**:e2206121.
46. Zhou ZG, Liu Y, Song W, Jiang X, Deng ZA, Xiong W, et al. Metabolic reprogramming mediated PD-L1 depression and hypoxia reversion to reactivate tumor therapy. *J Control Release* 2022;**352**:793−812.
47. Zhang RN, Yang YJ, Dong WJ, Lin MG, He J, Zhang XC, et al. D-Mannose facilitates immunotherapy and radiotherapy of triple-negative breast cancer *via* degradation of PD-L1. *Proc Natl Acad Sci U S A* 2022;**119**:e2114851119.
48. Herzig S, Shaw RJ. AMPK: guardian of metabolism and mitochondrial homeostasis. *Nat Rev Mol Cel Biol* 2018;**19**:121−35.
49. Lee H, Zandkarimi F, Zhang YL, Meena JK, Kim J, Zhuang L, et al. Energy-stress-mediated AMPK activation inhibits ferroptosis. *Nat Cel Biol* 2020;**22**:225−34.
50. Zhang WX, Pan XH, Xu YJ, Guo HJ, Zheng MM, Chen X, et al. Mevalonate improves anti-PD-1/PD-L1 efficacy by stabilizing CD274 mRNA. *Acta Pharm Sin B* 2023;**13**:2585−600.
51. Lee YH, Park HI, Chang WS, Choi JS. Triphenylphosphonium-conjugated glycol chitosan microspheres for mitochondria-targeted drug delivery. *Int J Biol Macromol* 2021;**167**:35−45.
52. Jiang MX, Zeng J, Zhao LP, Zhang MG, Ma JL, Guan XW, et al. Chemotherapeutic drug-induced immunogenic cell death for nanomedicine-based cancer chemo-immunotherapy. *Nanoscale* 2021;**13**:17218−35.
53. Zhou MX, Wang JX, Pan JX, Wang H, Huang LJ, Hou B, et al. Nanovesicles loaded with a TGF-β receptor 1 inhibitor overcome immune resistance to potentiate cancer immunotherapy. *Nat Commun* 2023;**14**:3593.
54. Blair AB, Wang J, Davelaar J, Baker A, Li K, Niu N, et al. Dual stromal targeting sensitizes pancreatic adenocarcinoma for anti-programmed cell death protein 1 therapy. *Gastroenterology* 2022;**163**:1267−80.
55. Koikawa K, Kibe S, Suizu F, Sekino N, Kim N, Manz TD, et al. Targeting Pin1 renders pancreatic cancer eradicable by synergizing with immunochemotherapy. *Cell* 2021;**184**:4753−71.